CrystEngComm

ROYAL SOCIETY OF CHEMISTRY

PAPER

View Article Online
View Journal | View Issue

Cite this: *CrystEngComm*, 2023, **25**, 1782

A quaternary solid-form of ritonavir: an oxalate salt oxalic acid co-crystal acetone solvate†

Chang Wang,[ab] Thomas D. Turner, ‡*[a] Cai Y. Ma,[a] Christopher M. Pask,[c] Ian Rosbottom,[a] Richard S. Hong,[d] Ahmad Y. Sheikh,[d] Qiuxiang Yin[b] and Kevin J. Roberts[a]

Ritonavir has been reported in seven crystal forms notably form I, II, IIIb and IV, as well as a hydrate, an L-tyrosine co-crystal and a formamide solvate. A new form is reported here with a novel quaternary structure with ritonavir as an oxalate salt, oxalic acid co-crystal and acetone solvate in a 1 : 1 : 0.5 : 0.5 stoichiometry. The new oxalate salt form (CCDC deposition number 2009282), was co-crystallised with oxalic acid from a supersaturated acetone solution, and exhibits a polar monoclinic crystal structure with a blocky needle-like crystal habit. The molecular conformation of ritonavir for the new form shows significant differences with respect to the well-characterised form I, II and IIIb polymorphs. Its crystallography is characterised by a 2-fold screw axis along the *b* axis, in a structure that exhibits multiple hydrogen bonds formed between amide–ureido, oxalate–oxalic acid and amide–amide groups in a layered intermolecular packing structure. Intermolecular stacking of the benzene and thiazole rings takes place along the crystallographic *a* axis with the needle axis growth of the crystals being likely to be governed by these interactions. The oxalate salt form co-crystal is found to have the characteristic conformations of the *N*-methyl urea and carbamate groups being in a *trans* and *trans* conformation respectively, as is the case for the recently discovered form IIIb, but in distinct contrast to *cis* and *trans* for form I, and *trans* and *cis* for form II. This may suggest that a *cis* and *cis* conformation for another new form may be feasible. The recovery of the form IV crystals at the lower concentrations of oxalic acid is perhaps indicative of its close similarity with the new oxalate salt co-crystal solvate form presented here.

Received 1st December 2022,
Accepted 14th February 2023

DOI: 10.1039/d2ce01612e

rsc.li/crystengcomm

Introduction

Ritonavir (Fig. 1) is a protease inhibitor for the treatment of acquired immunodeficiency syndrome (AIDS); the material's unexpected polymorphic transformation and resulting stability issues were well-documented two decades ago.[1,2] Ritonavir was found to exhibit poor aqueous solubility and is consistent with a class 4 molecule under the biopharmaceutics classification system (BCS), and hence was marketed either as an oral liquid or as semi-solid capsules in ethanol/water based solutions. This formulation strategy and the propensity for polymorphism in organic materials[3] provided an enhanced risk for the materials' transformation into a more stable and potentially more insoluble solid-form with time,[4–6] and some two years after its release, ritonavir was found to fail its dissolution testing specification due to the presence of a new and more stable form (form II) being precipitated within the formulated product.[1]

The structures of the form I and II polymorphs were determined and thoroughly characterised by Bauer *et al.*[1] The conformational energy landscape of the ritonavir molecule was modelled using density functional theory (DFT) by Chakraborty *et al.*,[7] highlighting that the identified molecular structure in its global minimum conformation exhibits stacking of its two thiazole rings. However, the conformational structures[1] for molecules from both forms I and II were not found to adopt the global minimum molecular conformation when the molecules were packed within their crystallographic structures. This suggested that the unfavourable molecular conformational energy is offset by the formation of inter-molecular interactions once packed into the 3-D lattices for forms I and II. Additionally the form

[a] *Centre for the Digital design of Drug Products, School of Chemical and Process Engineering, University of Leeds, Woodhouse Lane, Leeds, LS2 9JT, UK. E-mail: t.d.turner@leeds.ac.uk*
[b] *School of Chemical Engineering and Technology, State Key Laboratory of Chemical Engineering, Tianjin University, Tianjin 300072, China*
[c] *School of Chemistry, University of Leeds, Woodhouse Lane, Leeds, LS2 9JT, UK*
[d] *Solid State Chemistry, Process R&D, AbbVie Inc., North Chicago, IL, 60064, USA*

† Electronic supplementary information (ESI) available. CCDC 2009282 contains the supplementary crystallographic data for this paper. For ESI and crystallographic data in CIF or other electronic format see DOI: **https://doi.org/10.1039/d2ce01612e**

‡ School of Chemistry, University of Leeds, Woodhouse Lane, Leeds, LS2 9JT, UK.

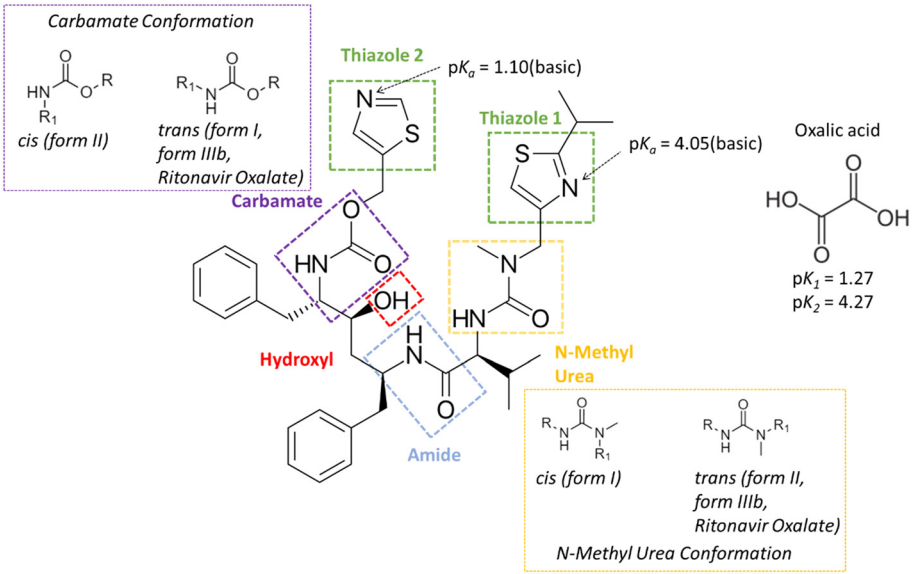

Fig. 1 The molecular structure of ritonavir and oxalic acid, highlighting the major functionalities within the molecular confirmation of the ritonavir molecule, together with their calculated (DFT in this work) acid dissociation constants.

I conformation has been found to adopt a *trans*, *cis* conformation for its carbamate and *n*-methyl urea groups respectively whereas form II has been found to adopt a *cis*, *trans* conformation of the same groups.

High-throughput polymorph screening by Morissette *et al.*[8] revealed (see Table 1) the existence of two new solvates (forms IIIa and V) as well as a further (metastable) phase (form IV), but up to now their full crystal structures have not been reported, albeit recent work[9] through melt crystallisation has now resulted in a further solid form with its crystal structure (form IIIb,[10] see Table 1). In this respect, due to the form III nomenclature being claimed for both the form identified from screening[8] and that recently crystallised from the melt,[9] for clarity we have referred to these two structures herein after as forms IIIa and IIIb, respectively. Surprisingly, due to its flexible molecular conformation and glass-forming tendency of the material, only a single co-crystal form of ritonavir co-crystallised with L-tyrosine have been reported.[11–13] More recently, Wang *et al.*[14] have characterised and compared, in significant detail, the crystal chemistry for both forms I and II in terms of their molecular conformations, polarizabilities, hydrogen bonding networks, intermolecular packing structures and crystal morphologies cross-correlating these to a wider assessment of their crystallisability behaviour and respective surface properties.

Generally, a selected co-former can be incorporated into the crystal lattice with molecules of charged or uncharged active pharmaceutical ingredients (API) when a salt or co-

Table 1 A summary of the known structural data of the crystal forms of ritonavir from this and previous studies together with the associated preparative methods. To date form II has been found to be the most stable form of ritonavir. Form IV here is the same structure but in this study was prepared *via* a different methodology to previously reported work

Form	Crystal system	Solid-state structure	Melting point (°C)	Crystallisation method	Single crystal structure	Molecular Conformation[a]	References
I	Monoclinic	Anhydrous pure form	123	Ethanol/H_2O	Y	*trans* and *cis*	1
II	Orthorhombic	Anhydrous pure form	126	Ethanol/H_2O	Y	*cis* and *trans*	1
IIIa	Monoclinic	Formamide solvate	78–82	Formamide/toluene or formamide/butyl acetate or formamide/acetone	N	Unknown	8
IIIb	Monoclinic	Anhydrous pure form	114.6	Melt	Y	*trans* and *trans*	10
IV	Unknown	Anhydrous pure form	116	Acetonitrile/butyl acetate or acetonitrile/isobutyl acetate or acetonitrile/isopropyl acetate	N	Unknown	8
IV	Unknown	Anhydrous pure form	121.8	Acetone/oxalic acid	N	Unknown	(This study, 2023)
V	Monoclinic	Trihydrate	97	Aqueous slurry conversion from III (readily transforms to I)	N	Unknown	8
	Unknown	L-Tyrosine co-crystal	112.9	1 : 1 liquid assisted grinding with methanol : water (1 : 1)	N	Unknown	13
	Monoclinic	Salt co-crystal solvate	125.3	Acetone/oxalic acid	Y	*trans* and *trans*	(This study, 2023)

[a] Refers to the molecular conformation with respect to the carbamate and *N*-methyl urea groups.

crystal, respectively, is formed.[15–17] To distinguish between whether a salt or a co-crystal might form, the difference in pK_α between the API and the co-former usually provides a useful guide to predict the possibility of proton transfer during the co-crystallisation process ($\Delta pK_\alpha = pK_{\alpha(API)} - pK_{\alpha(co\text{-}former)}$). It is generally accepted[18,19] that a non-ionised co-crystal complex would more likely to be formed when the magnitude of $\Delta pK_\alpha \leq 0$, although this has been recently refined <-1 through examination of >6000 molecules within the Cambridge Structural Database (CSD).[20] In contrast, when the $\Delta pK_\alpha > 4$ it would be expected that any resultant solid-form would most likely form a salt.[20] For the borderline region with ΔpK_α (0–3), it is not generally regarded that predictive methods can accurately evaluate whether a co-crystal or salt form will be produced. Ritonavir has reported $pK_{\alpha1}$ and $pK_{\alpha2}$ values of 1.9 and 2.5 for the two thiazole groups,[21] whilst the pK_α values of oxalic acid have been found to be 1.27 and 4.27 for $pK_{\alpha1}$ and $pK_{\alpha2}$, respectively.[22]

Reflecting its small molecular size and large number of hydrogen bond accepter/donor options, oxalic acid (Fig. 1) is a good co-former to access potentially novel co-crystal solid forms. In the case of its use as a co-former for ritonavir, the ΔpK_α values are 0.63 and 1.23 with the two thiazole groups, respectively. Given the high propensity of potential H-bond donors and acceptors in ritonavir,[14,23] its NH and C═O functional groups offer the most likely options for the formation of intermolecular H-bonds with co-formers.

In this paper, the crystallisation of ritonavir in the presence of oxalic acid has been explored with the aim to further examine its solid-form landscape. The work also builds upon our recent in-depth examination of the solid-state and surface properties of forms I and II,[14] their intermolecular hydrogen bonding networks and how these various solid forms relate to the molecular conformation in the solid-state.

Experimental section

Materials

Ritonavir form II was obtained from AbbVie Inc. and used as received without further purification. Anhydrous oxalic acid (>99.0%) was purchased from Sigma Aldrich, acetone HPLC grade (>99%) was used as supplied by VWR International.

Methods

Crystallisation experiments. Solutions of ritonavir in acetone solution were prepared at a concentration of 90 mg ml^{-1} in the presence and absence of oxalic acid (molar ratio $m_{oxalic\ acid}/m_{ritonavir} = 2:5$ was chosen due to the di-acid nature of oxalic acid, however the impact of oxalic acid concentration was not extensively investigated here). The composition was heated to ensure complete dissolution of solids and agitated with a magnetic stirrer at 700 rpm. 10 ml aliquots of solution were then filtered into 20 ml vials through a 0.45 μm filter membrane.

The solutions were subsequently used for both slow evaporative and fast cooling crystallisation experiments. For the former case the vials were sealed with parafilm which were perforated with several small holes in order to ensure slow evaporation (not to dryness) at room temperature (~25 °C). For the latter case, the vials were sealed and quench cooled to 5 °C to achieve high supersaturations.

In both the above cases, the resulting crystals were filtered and dried after solvent evaporation with the solid phase being analysed using a differential scanning calorimeter with samples contained in a loosely covered aluminium pan using a sample weight of 2–5 mg and a heating rate of 10 °C per minute and a nitrogen flow of 40 mL min^{-1} (DSC) (Mettler-Toledo DSC-1), Olympus optical microscope and powder X-ray diffraction (PXRD, Bruker D8 diffractometer, Cu K_α 1.54 Å).

Crystal structure determination. An isolated single crystal was selected and mounted on a nylon loop using inert oil. Single crystal crystallographic measurements were carried out at 150 K on a Rigaku SuperNova diffractometer equipped with an Atlas CCD detector and connected to an Oxford Cryostream low temperature device using mirror monochromated Cu K_α radiation (λ = 1.54184 Å) from a Microfocus X-ray source. The crystallographic structure of the crystal was solved by intrinsic phasing using SHELXT[24] and refined by a full matrix least squares technique based on $|F|^2$ using SHELXL2014.[25]

Computed pK_α values. Computed pK_α values of all heteroatoms were first determined using the ACD (Advanced Chemistry Development Inc.) Suite software (version 12.0). The micro-pK_α values of the thiazole nitrogens were then determined and refined using density functional theory (DFT) calculations implemented through the Jaguar DFT and pK_α suite,[26,27] where the micro-pK_α, defined as the pK_α of a specified atom, is predicted through a thermodynamic cycle considering the DFT energies of both the protonated and non-protonated forms in vacuum and water. Conformational sampling of both the neutral and protonated structures for ritonavir was performed using the OPLS4 force field as implemented in the MacroModel program.[28,29] The top 10 conformations were then optimized using B3LYP/6-31G**.[30,31] Afterwards, single point calculations were performed using B3LYP/cc-pVTZ.[32] Implicit water was considered using the PBF solvation model.[33] The DFT predicted pK_α values were performed in implicit water such that the predicted values can be referenced against the ΔpK_α rule, which utilizes pK_α values from aqueous media.[20] However, we acknowledge that the proton transfer experimentally occurs in either the crystalline environment or in acetone. A future study in assessing the computed interaction energies of multiple salt and co-crystal pairs may be informative.

Results and discussion

Solid form characterisation

Form I was found to consistently crystallise when no oxalic acid was added to the supersaturated solutions, independent

of the crystallisation method. However, microscopy analysis of the crystals harvested from the slow-solvent evaporation experiments in the presence of 5% oxalic acid, revealed a distinctly plate-like morphology (Fig. 2(i)) which was rather similar to that previously reported for form IV.[8] However, with an increasing concentration of oxalic acid, a more block-like or tabular morphology (Fig. 2(ii)) was obtained from both the evaporative and rapid cooling crystallisation experiments.[34]

Analysis of the PXRD patterns recorded from powdered samples of the crystals, as shown in Fig. 3, reveals distinct differences. The plate-like crystals exhibited characteristic diffraction peaks at 2θ values of 3.21°, 6.13°, 6.87°, 7.98° and 10.04° consistent with those of form IV.[8,35] In contrast, the tabular crystals were found to exhibit characteristic peaks at 5.24°, 6.32°, 6.93°, 8.67° and 11.66°, which were not consistent with any of the previously observed solid forms as shown in Table 1 and hence were found to be consistent with the existence of a new form, which was found to be a ritonavir oxalate oxalic acid co-crystal acetone solvate, hereinafter for brevity "oxalate salt form".

DSC analysis of the crystals of form IV and oxalate salt form (Fig. 4) revealed that the form IV data only exhibited one endothermic melting peak at about 121.8 °C which is close to that of 116 °C reported in the literature.[8,35] The difference perhaps reflects variations in heating rate, crystal size and the DSC instrument precision between the data reported here and previous work. Analysis of the oxalate salt form crystals revealed two endothermic peaks at 47.8 and 125.3 °C, respectively. The first very small endothermic peak at 47.8 °C, being close to the boiling point of acetone (boiling point 56 °C), would be consistent with the removal of weakly bound surface solvent, most likely to be acetone due to the crystallisation conditions, and not crystallographically bound due to the very small peak area. The second endotherm at 125.3 °C would be more indicative of melting of the material.

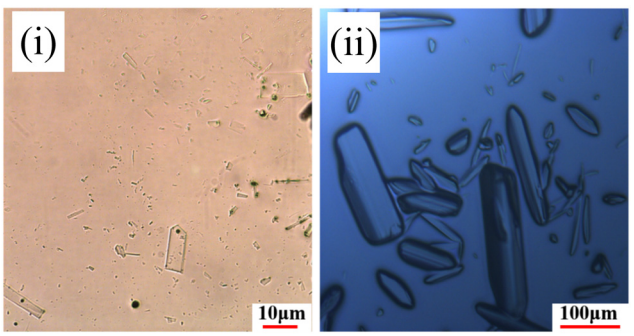

Fig. 2 Optical micrographs from the ritonavir re-crystallisation experiments from supersaturated acetone solutions in the presence of oxalic acid showing the formation of form IV (i) and the new oxalate salt form (ii), highlighting the different crystal habits of the two forms.

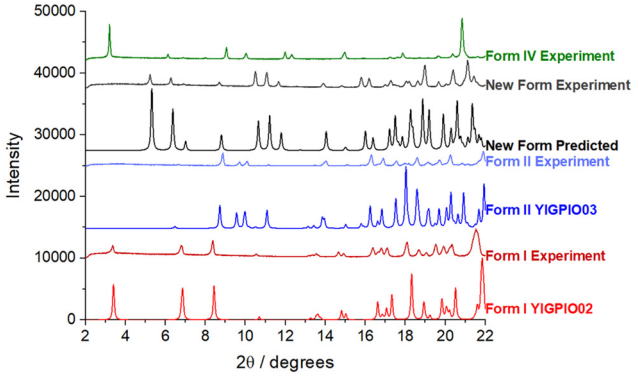

Fig. 3 PXRD patterns of ritonavir polymorphs, I, II, IV and the new oxalate salt form.

Crystal structural determination

The crystal size of the isolated form IV crystals were unfortunately not found to be sufficiently large enough for a full single crystal diffraction analysis, and hence only the much larger single crystals of the salt form crystals were examined.[34] Examination of optical micrographs of the single crystal selected for crystallographic analysis (see Fig. S2 in ESI†) revealed a crystal habit elongated along its crystallographic *a* axis.

A more detailed analysis of the crystal structure of the new oxalate salt form revealed it to crystallise in a polar monoclinic structure encompassing a quaternary ritonavir oxalate salt oxalic acid co-crystal acetone solvate with a 1 : 1 : 0.5 : 0.5 stoichiometry *i.e.* with one ritonavir cation, one oxalate anion, one half molecule of acetone and one half molecule of oxalic acid, within the asymmetric unit (Fig. 5) and with the latter two being disordered but centred approximately at the same lattice site. The associated

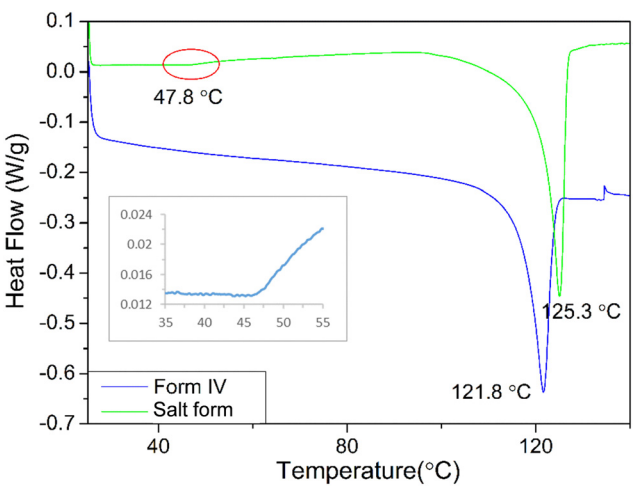

Fig. 4 DSC thermograms of ritonavir revealing the melting points for form IV and the new oxalate salt form with the latter revealing a possible evaporation of surface-bound solvent occurred in the salt solvate at about 47.8 °C. The inset shows an enlargement of the feature at 47.8 °C.

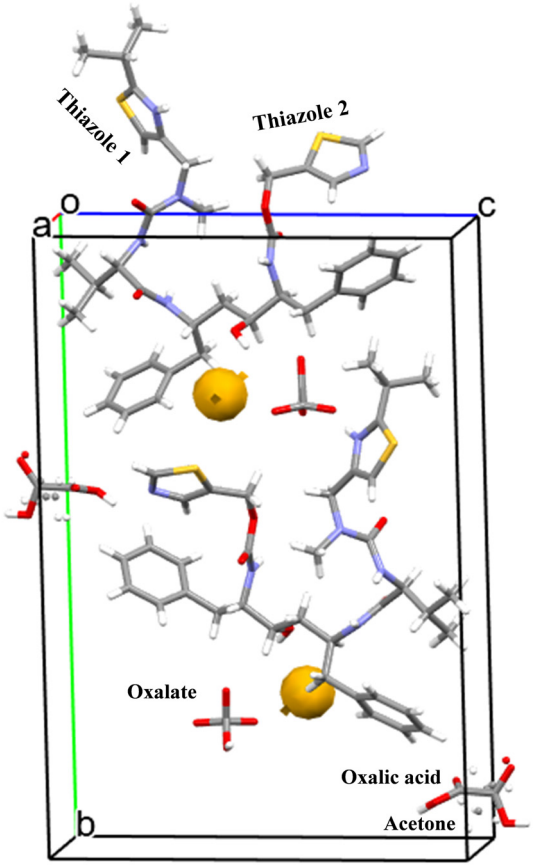

Fig. 5 The unit cell of the new oxalate salt form which contains two ritonavir cations, two oxalate anions together with one oxalic acid molecule and one acetone molecule, and also the void space (0.3% as shown in Table 2).

crystallographic data are given in Table 2 and the unit cell shown in Fig. 5.

As shown in Fig. 5, the growth morphology is actually dominated by stacking of the benzene and thiazole groups in the oxalate salt form along the crystallographic *a* axis, which is unusual considering the stronger ionic salt interactions were found to be formed in the *b*, *c* directions. This might suggest salt formation to be the likely initial driver for the nucleation of this solid form which allows the molecules to assemble for subsequent orientation followed by stacking of the salt dimer/tetramer dominating the growth process.

The molecular and crystal structural descriptors and some thermodynamic data for forms I and II[1,14] and IIIb[9] together with the new oxalate salt form structure from this study are provided in Table 2. Previous work[9] has shown that form IIIb has a higher molecular volume (Table 2), a higher crystal structure density and a lower void space when compared to the less close-packed form II structure. In this study, the new oxalate salt form was found to have the highest crystal density (1.33 g cm^{-3}) of all these four solid-forms with the lowest void space and highest packing efficiency. The lowest calculated surface area of ritonavir molecule in the oxalate salt form when compared to other three forms, may be attributed to the "stacking" molecular structure shown in Fig. 6 (see also Fig. S4 in the ESI†). Like other conformational polymorphs of complex pharmaceutical molecules, these observations are likely to reflect the result of interplay between the relative strength of the intermolecular and intramolecular energies.[36]

Conformational analysis

The molecular conformation of ritonavir within the new oxalate salt form salt-solvate structure was found to be significantly different from that of forms I, II and IIIb. In the oxalate salt form, the ritonavir molecule is torsioned such to make the two thiazole rings closer to each other (Fig. 6 and see also Fig. S4(ii) in the ESI†) which is much closer to the

Table 2 Characteristic molecular descriptors and crystallographic structural data for the ritonavir polymorphs (forms I, II, IIIb and oxalate salt form)

Material descriptor	Form I	Form II	Form IIIb	Oxalate salt form[(this study)]
Refcode	YIGPIO02[1]	YIGPIO03[1]	YIGPIO04[9]	2009282[Deposition no.]
Molecular volume (Å^3)	721.24	676.74	678.58	695.73[a] (870.51[b])
Molecular weight (g mol^{-1})	720.94	720.94	720.94	720.94[a] (885.03[b])
Molecular surface area (Å^2)	656.46	645.09	634.94	617.51[a] (717.47[b])
Melting point (°C)	123[1]	126[1]	114.6[9]	125.3
Space group	$P2_1$[1]	$P2_12_12_1$[1]	$C2$[9]	$P2_1$
Z/Z'	2/1[1]	4/1[1]	4/1[9]	2/1
a (Å)	13.433(1)[1]	10.0236(3)[1]	23.3307(19)[9]	5.2615(2)
b (Å)	5.293(2)[1]	18.6744(4)[1]	4.9511(5)[9]	25.2098(9)
c (Å)	27.092(4)[1]	20.2692(7)[1]	33.638(3)[9]	16.6111(6)
α (°)	90[1]	90[1]	90[9]	90
β (°)	103.102(9)[1]	90[1]	91.274(6)[9]	91.994(3)
γ (°)	90[1]	90[1]	90[9]	90
Cell volume (Å^3)	1876.0(8)[1]	3831.5(2)[1]	3884.6(6)[9]	2201.99(14)
Packing coefficient	0.77	0.71	0.714[9]	0.79
Void space (%)	0.8	1.0	0.36[9]	0.3
Density (g cm^{-3})	1.28[1]	1.25[1]	1.325[9]	1.33

Note that void space (%) based on probe radius: 1.0 Å & approximate grid spacing: 0.5 Å. Average packing coefficient for organic crystals: 0.68. [a] Calculated with ritonavir molecule only. [b] Based on molecules in the symmetric unit (1 ritonavir, 1 oxalate, 0.5 acetone and 0.5 oxalic acid).

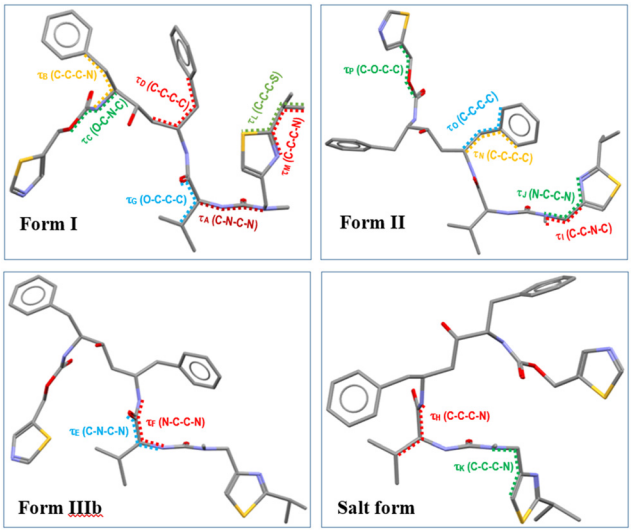

Fig. 6 The different molecular conformations of ritonavir in form I, form II, form IIIb and oxalate salt form.

global minimum conformation "f" calculated by Chakraborty *et al.*[7] Examination of the four torsion angles (τ_E, τ_F, τ_G, τ_H) involving the rotation of the molecular fragment containing the phenyl–hydroxyl–phenyl–carbamate–thiazole_1 groups, highlights that the new oxalate salt form conformer reveals the molecule to be "folded" into a "U" shape (see Fig. S4(i) in the ESI†). The folded conformation is likely stabilized through intra-molecular dispersive interaction. This is likely due to the polar nature of the crystal structure, resulting in hydrophobic collapse of the ritonavir conformation, where its hydrophobic substituents are shielded through intra-molecular interactions. It was found that the angles of these four torsions in forms I, II and IIIb have differences in the range of 3–20° (see Table S1 in the ESI†), which are quite small. However, when comparing the conformation of the new oxalate salt form with the other three forms (I, II and IIIb), the torsional angle differences of τ_E, τ_F, τ_G and τ_H become much larger (see Fig. S4(i) and S5 in the ESI†), to a range of 164–165°, 174–178° and 158–162° with regard to form I, form II and form IIIb (see Table S1 in the ESI†), respectively.

As shown in the literature,[1,9,14] the main molecular conformational differences between the polymorphic forms can be characterised with respect to the ideal conformations around the *N*-methyl urea and the carbamate functional groups. In this, form I has a *cis N*-methyl urea conformation and a *trans* carbamate conformation respectively, whilst form II has a *trans N*-methyl urea conformation and a *cis* carbamate conformation. This is caused by the differences between the torsion angles between form I and II: τ_A and τ_C being 170.6° and 175.5°,[14] respectively (see Fig. S7(i) and Table S1 in the ESI†), leading to the R_1 (Fig. 1) of the *cis* and *trans* configurations orientated in opposite directions. As shown in Table 3 (see also Fig. S7(ii) in the ESI†), the torsion angle τ_A of the oxalate salt form (170.6°) is very close to that of form II and form IIIb with only 5° and 6.4° differences respectively, consistent with the *N*-methyl urea conformation being in a *trans* configuration for the form IIIb and the new oxalate salt form (see Fig. S7(vi) in the ESI†). The differences of τ_C between the oxalate salt form (−171.6°) and forms I/IIIb (see Fig. S7(iii and vi) in the ESI†) were found to be only 9.7° and 14.7° respectively, and hence the oxalate salt form has a *trans* carbamate conformation (Table 3 and see Fig. S7(i) in the ESI†). Therefore the molecular structures of the form IIIb and oxalate salt form have both these groups in the *trans* configurations comparing to *cis* and *trans* conformation in form I, and *trans* and *cis* conformation in form II. The detailed comparisons of torsion angles (τ_A, τ_B, τ_C, τ_D) between forms I, II, IIIb and the new oxalate salt form are shown in the ESI† (see Fig. S7 and Table S1).

There are also additional torsion angles which were found to exhibit large differences between these four forms and these are plotted in Fig. S5 and listed in Table S1 (ESI†). By comparing the torsions (τ_I, τ_J, τ_K) in the molecular structure of the oxalate salt form with forms I, II and IIIb, it was found that only τ_I in the oxalate salt form is close to form I with a small (21°) angular difference, but all three torsions (τ_I, τ_J, τ_K) in both form IIIb and oxalate salt form also have small (<33°) angular differences. For the torsions (τ_L, τ_M), the isopropyl group in the oxalate salt form rotates about (105–111°), (170–178°) and (102–112°) compared to these in forms I, II and IIIb, whilst the torsions (τ_N, τ_O) have about a (160–180°) angle of rotation. Interestingly, as shown in Table 3 (see also Fig. S7(iii) in the ESI†), the ureido and thiazole 1 functional groups are roughly overlaid between form IIIb and new oxalate salt form. However, the rest of the molecular structures of both forms rotate about 160° to each other as evidenced by the torsion angle τ_E in Table 3. Further detail can be found in ESI.†

Table 3 The torsion angles (in degrees) of 5 torsions (τ_A, τ_B, τ_C, τ_D, τ_E) and their differences between the new oxalate salt form and forms I, II and IIIb

Torsion	(a) Form I	(b) Form II	(c) Form IIIb	(d) Salt form	Δ(a–b)	Δ(a–d)	Δ(b–d)	Δ(c–d)
τ_A	−23.8	165.6	177.0	170.6	170.6	165.6	5.0	6.4
τ_B	71.0	−72.8	46.1	48.5	143.8	22.5	121.3	2.4
τ_C	178.7	−5.8	173.7	−171.6	175.5	9.7	165.8	14.7
τ_D	55.9	168.3	173.3	−175.4	112.4	128.7	16.3	11.3
τ_E	−67.7	−56.8	−73.9	127.5	10.9	164.8	175.7	158.6

Note that the definitions of 4 torsion angles for form I, form II, form IIIb and the new oxalate salt form can be found in Fig. 6.

Hydrogen bonding network analysis

Ritonavir has a relatively large molecular mass compared to many API's, exhibiting four hydrogen bond donors; one hydroxyl O–H and three amidic N–H groups together with twelve acceptors.[14] In the oxalate salt form structure, the hydrogen bond donors and acceptors of ritonavir are in competition with those provided by oxalic acid during co-crystallisation. Hence, its resulting crystal structure encompasses donor–acceptor interactions between API/API, API/co-former and co-former/co-former. Details on the hydrogen bonds and their structure for the ritonavir polymorphs for form I, form II, form IIIb and the new oxalate salt form are presented in Table 4. Examination of the data reveal that there are four hydrogen bonds formed between adjoining ritonavir molecules in the crystal structures of forms I, II and IIIb with forms I and IIIb having their hydrogen bonding donors and acceptors from the exactly same functional groups but with different bond lengths. However, there are only three hydrogen bonds formed within the new oxalate salt form structure with the intermolecular hydrogen bonds involving the hydroxyl group present in forms I, II and IIIb being absent in the new oxalate salt form structure. However, these are replaced by O–H (hydroxyl)···O (oxalate) interactions at a similar inter-atomic distance. The thiazole 2 acceptor N forms a hydrogen bond with one of the hydroxyl groups in the oxalic acid. N–H (ureido) switched its acceptor from O (ureido) in form I/IIIb or O (carbamate) in form II to O (amide). Hence both N–H (amide) and N–H (ureido) in the new form act as hydrogen bond donors to the O (amide) acceptor. In contrast the corresponding O (ureido) hydrogen bonds to one of the oxalic acid hydroxyl groups. A new donor: N–H^+ (thiazole 1) forms the ionic salt interaction with the other O^- ion in the oxalate molecule.

The N3–H3A (amide)···O4 (amide), N4–H4 (ureido)···O4 (amide) and N2–H2 (carbamate)···O2 (carbamate) hydrogen bonds of ritonavir and the O9–H9A (oxalate)···$O6^-$ (oxalate) hydrogen bond (with the shortest bond length of 1.635 Å), as shown in Fig. 7 and summarised in Table 4, form the layered 2D hydrogen-bonding network structure with stacking in the *a* axis direction. It would be expected that the strong stacking structure involving 4 hydrogen bonds would lead to fast crystal growth in the *a* axis direction. The chain hydrogen bonding structures with ritonavir and the oxalate in the *b* axis direction, and ritonavir and the oxalic acid in the *c* axis direction would produce similar growth rates but slower than the *a* axis direction. This would be consistent with the crystallisation of block-like crystals; similar to those shown in Fig. 2.

Overall, three functional groups (amide, ureido and carbamate) of ritonavir form three hydrogen bonds with another ritonavir molecule with the oxalate ion also forming one hydrogen bond with another molecule of itself in the same *a* axis direction, leading overall to a 2D hydrogen bonding network. The oxalate also acts as an acceptor forming two hydrogen bonds with the hydroxyl and thiazole 1 groups of two separate ritonavir molecules in the *b* axis direction, whilst the oxalic acid donates hydrogens to both the ureido and thiazole 2 groups from two separate ritonavir molecules to form two hydrogen bonds in the *c* axis direction. Hence, a chain hydrogen bonding network is formed in both the *b* and *c* axis directions.

Crystal chemistry and local coordination within the quaternary structure

Ritonavir cation. Based on the previous study, ritonavir form II has four functional groups (amide, ureido, carbamate

Table 4 Comparison between the geometric parameters for the hydrogen bonds present in the form I, form II, form IIIb and new oxalate salt form polymorphs; highlighting the hydrogen to acceptor and donor to acceptor distances and the bond angle (θ). Note that the atom labelling of hydrogen bonds and their distributions in the new oxalate salt form can be found in Fig. S6 (ESI,† section S4)

	Hydrogen bond					
Compound	Donor (D–H)	···	Acceptor (A)	*d* (H···A) (Å)	*d* (D···A) (Å)	θ (°) (D–H···A)
Form I[1]	N–H (amide)	···	O (amide)	1.960	3.029(6)	160.3
	N–H (ureido)	···	O (ureido)	2.222	3.275(8)	157.5
	N–H (carbamate)	···	O (carbamate)	2.131	3.261(6)	148.1
	O–H (hydroxyl)	···	N (thiazole 2)	2.141	2.989(6)	131.0
Form II[1]	N–H (amide)	···	O (hydroxyl)	2.245	2.999(6)	146.2
	N–H (ureido)	···	O (carbamate)	2.122	2.933(6)	157.0
	N–H (carbamate)	···	O (amide)	2.219	2.883(6)	134.0
	O–H (hydroxyl)	···	O (ureido)	1.900	2.688(5)	160.7
Form IIIb[9]	N–H (amide)	···	O (amide)	1.946	2.773(12)	160.9
	N–H (ureido)	···	O (ureido)	2.120	2.963(2)	166.1
	N–H (carbamate)	···	O (carbamate)	1.972	2.800(14)	161.4
	O–H (hydroxyl)	···	N (thiazole 2)	2.252	3.049(16)	164.5
Oxalate salt form	N–H (amide)	···	O (amide)	2.390	3.390(5)	166.5
	N–H (ureido)	···	O (amide)	2.116	2.900(5)	151.2
	N–H (carbamate)	···	O (carbamate)	2.344	3.187(5)	167.1
	O–H (hydroxyl)	···	O (oxalate)	2.029	2.849(5)	179.9
	N–H^+ (thiazole 1)	···	O^- (oxalate)	1.810	2.664(5)	171.6
	O–H (oxalate)	···	O^- (oxalate)	1.635	2.443(5)	167.9
	O–H (oxalic acid)	···	O (ureido)	1.703	2.506(9)	166.3
	O–H (oxalic acid)	···	N (thiazole 2)	1.983	2.604(10)	132.0

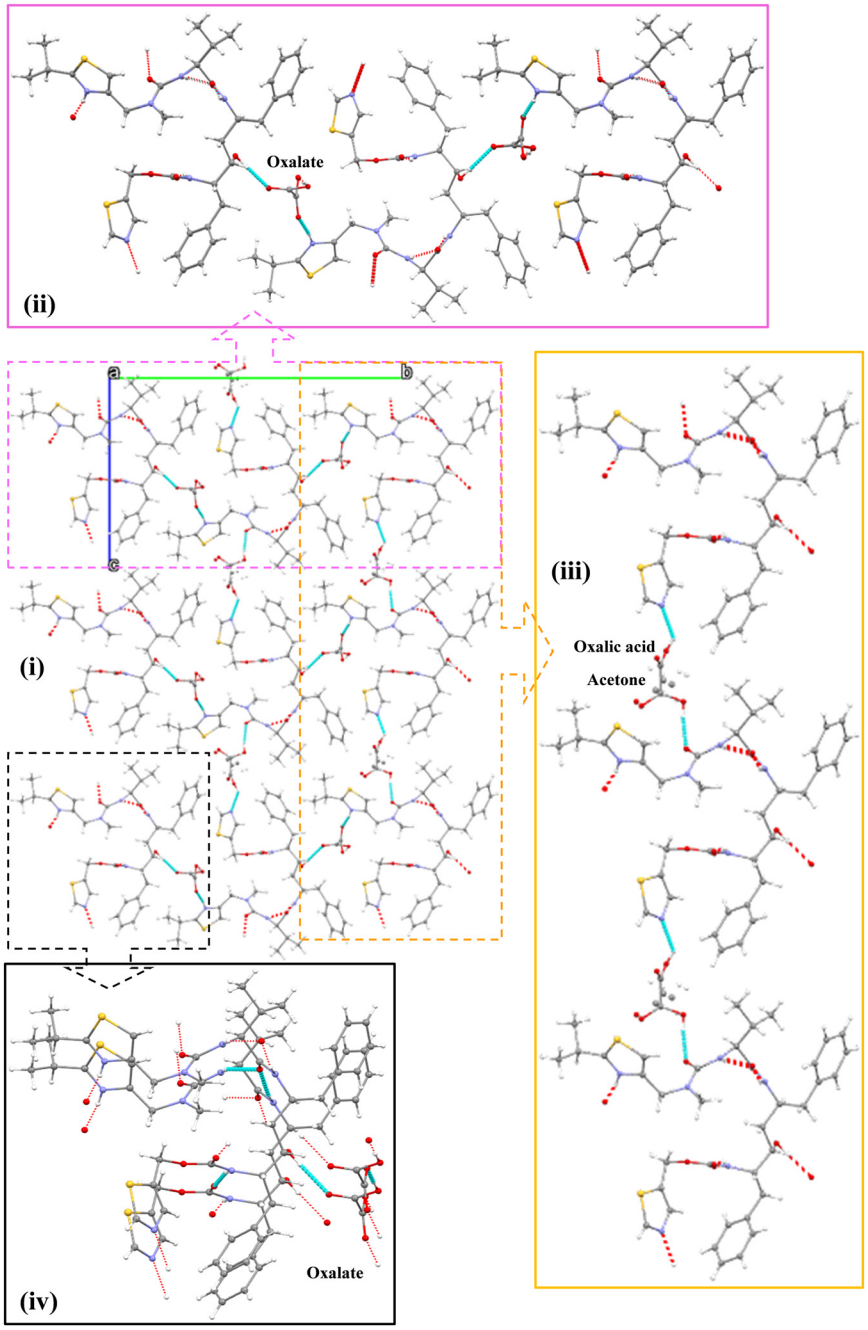

Fig. 7 The chain structure between ritonavir and the oxalate ions within the new oxalate salt form crystal structure, which extends down the *a* axis (i), highlighting the different linkages between oxalic acid and ritonavir: hydrogen bonding chain networks in *b* axis direction (ii) and *c* axis direction (iii), and the ritonavir stacking with hydrogen bonding 2D network in *a* axis direction (iv).

and hydroxyl) involved in hydrogen bonding interactions with one additional interaction (thiazole 2) for form I. In the new oxalate salt form polymorph, one further functional group (thiazole 1) and also both the oxalate (OX A) ion and oxalic acid (OX B) contribute to the formation of hydrogen bonds. As shown in Table 4 (see also Fig. S6 in the ESI†), oxygen in the amide group acting as an acceptor binds to both the amide and ureido groups of another ritonavir molecule through their N–H hydrogen donors. In addition, ureido also acts as an acceptor to bind with oxalic acid to form the O–H (OX B)···O (ureido) hydrogen bond. The carbamate group binds to carbamate of another ritonavir molecule through the N–H···O hydrogen bond. The hydroxyl and thiazole 1 groups from two separate ritonavir molecules donate hydrogens to the two oxygens in the oxalate, forming O–H (hydroxyl)···O (OX A) and N–H (thiazole 1)···O (OX A) hydrogen bonds. The oxalate also has a hydrogen bond (O–H···O) with another oxalate in the *a* axis direction. The oxalic acid only acts as hydrogen donors to ureido and thiazole 2 from two separate ritonavir molecules, hence forming O–H

(OX B)···O (ureido) and O–H (OX B)···N (thiazole 2) hydrogen bonds. Of the disordered oxalic acid and acetone molecules (both centered at approximately the same lattice site), acetone was not found to have any hydrogen bonding interactions with other molecules in the lattice.

Oxalic acid (oxalate anion and oxalic acid). The oxalic acid was found to interact with ritonavir *via* O (ritonavir O5)···OH (oxalic acid) and N (ritonavir N1)···OH (oxalic acid) hydrogen bonds to form a coplanar chain structure (Fig. 7(iii)). The oxalate interacts with ritonavir *via* a coplanar chain by OH (ritonavir)···O (carbonyl in oxalate) and NH^+ (thiazole 1)···O^- (carbonyl in oxalate) *via* an ionic interaction as shown in Fig. 7(ii) (see also Fig. S6 in the ESI†). The intermolecular O^- (oxalate)···OH (oxalate), O (ritonavir O2)···NH (ritonavir) and O (ritonavir O4)···NH (ritonavir) hydrogen bonds were found to be involved in the formation of a layered stacking structure which enables the formation of short π–π stacking interactions between the benzene and thiazole rings of ritonavir (Fig. 7(iv)). Such a strong inter-molecular stacking structure, which was found to take place along the *a* axis, would be consistent with the observed faster growth along the *a* axial direction (Fig. 5 (see also Fig. S2 in ESI†)).

The corresponding calculated pK_a values of the two thiazole groups in ritonavir (thiazole 1 = 4.05 and thiazole 2 = 1.10) as shown in Fig. 1, show that these weakly basic nitrogen atoms are the only groups in the molecule which are likely to form salt interactions with oxalic acid due to the ΔpK_a values being 2.78 and −0.17 respectively (further details in Table S3 (ESI†)). A recent study into >6000 acid–base pairs in the Cambridge Structural Database, provided convincing evidence that the $\Delta pK_a > 2$–3 rule, holds for the large majority of molecules and that there were three distinct regions; zone 1 $\Delta pK_a < -1$ where non-ionised hydrogen bonded pairs dominate the crystal structures, zone 2 ΔpK_a = −1 to 4 where a combination of non-ionised hydrogen bonded and salt complexes can form and zone 3 $\Delta pK_a > 4$ where the vast majority of crystal structures are salts.[20] Ritonavir when paired with oxalic acid falls into zone 2 of these categories and perhaps explains to some extent why ritonavir forms both a salt and co-crystal complex with oxalic acid.

Concluding remarks

In this paper, a new solid form of ritonavir (salt co-crystal solvate) was isolated through co-crystallisation with oxalic acid in supersaturated acetone solutions. Single crystal X-ray diffraction analysis reveals the molecular conformation of the new oxalate salt form structure to be associated with the folding of the ritonavir molecule, hence forming a stacking or "U" shape molecular structure similar to that predicted as the global minimum conformation.[7] This folding of the molecular conformation not only stabilizes the structure through intra-molecular dispersive interactions, but also exposes its polar atoms to be able to form strong, directional hydrogen bonding and ionic interactions. Both the *N*-methyl urea conformation and the carbamate conformation in the new oxalate salt form structure were found to be in a *trans* and *trans* conformation in contrast to *cis* and *trans*, and *trans* and *cis* for forms I and II, respectively.[14] This might, in turn, suggest that another new form might be feasible having *cis* and *cis* conformations, albeit there has been no direct evidence of this to date. However recent discovery of the structure of form IIIb,[9] also in a *trans* and *trans* conformation, may provide opportunities for further analysis in this regard. The new oxalate salt form co-crystal was also found to have the highest crystal density of all four polymorphs (I, II, IIIb and oxalate salt form) with known structures. There was no observed degradation of the sample upon heating with no obvious loss of structural solvent in the DSC traces. However, in future studies the possibility of removing the structural solvent from the solid-state during, for example, long term storage or at elevated temperatures, would reveal whether these types of materials have utility as pharmaceutical precursors. The crystal habit of the new oxalate salt form structure displays as a blocky-needle where the longer needle axis was found to be the short *a* crystallographic axis and corresponds to close π–π stacking of the benzene and thiazole rings along this lattice direction.

List of symbols and abbreviations

$a, b, c, \alpha, \beta, \gamma$	Crystal unit cell parameters
λ	Radiation wavelength
τ	Interatomic torsion angle of molecular fragment
Z/Z'	Number of molecules in the unit cell/asymmetric unit
AIDS	Acquired immunodeficiency syndrome
API	Active pharmaceutical ingredient
BCS	Biopharmaceutics classification system
DFT	Density functional theory
DSC	Differential scanning calorimetry
H-bond	Hydrogen bond
OX A	Oxalate
OX B	Oxalic acid
pK_a	Acid dissociation constant at logarithmic scale
PXRD	Powder X-ray diffraction
Å	Angstrom 10^{-10} m

Conflicts of interest

There are no conflicts of interest to declare.

Acknowledgements

One of us (C. W.) acknowledges funding support from the China Scholarship Council. This work was also supported by the Advanced Manufacturing Supply Chain Initiative 'Advanced Digital Design of Pharmaceutical Therapeutics' (ADDoPT) project (Grant No. 14060). This research also builds upon previous work on morphological modelling which was supported by EPSRC grant EP/I028293/1. We also gratefully

acknowledge EPSRC for the long-term support of crystallisation research at Leeds notably recently through the Critical Mass Project grant 'Molecules, Clusters and Crystals' (Grant references EP/IO14446/1 and EP/IO13563/1) which was in collaboration with the University of Manchester. Two of us (R. S. H. and A. S.) are employees of AbbVie and may own AbbVie stock. AbbVie contributed to the design of study; interpretation of data, and in reviewing, and approving of the final publication.

References

1 J. Bauer, S. Spanton, R. Henry, J. Quick, W. Dziki, W. Porter and J. Morris, *Pharm. Res.*, 2001, **18**, 859–866.
2 S. Chemburkar, R. J. Bauer, K. Deming, H. Spiwek, K. Patel, J. Morris and J. Quick, *J. Am. Chem. Soc.*, 2000, **4**, 413–417.
3 J. Bernstein, presented in part at the Engineering of Crystalline Materials Properties: State of the Art in Modeling, Design and Applications, *NATO Science for Peace and Security Series B-Physics and Biophysics*, Dordrecht, 2008.
4 W. Du, Q. Yin, H. Hao, Y. Bao, X. Zhang, J. Huang and J. Gong, *Ind. Eng. Chem. Res.*, 2014, **53**, 5652–5659.
5 A. Maher, D. M. Croker, Å. C. Rasmuson and B. K. Hodnett, *Cryst. Growth Des.*, 2012, **12**, 6151–6157.
6 A. Maher, D. M. Croker, C. C. Seaton, Å. C. Rasmuson and B. K. Hodnett, *Cryst. Growth Des.*, 2014, **14**, 3967–3974.
7 D. Chakraborty, N. Sengupta and D. J. Wales, *J. Phys. Chem. B*, 2016, **120**, 4331–4340.
8 S. L. Morissette, S. Soukasene, D. Levinson, M. J. Cima and O. Almarsson, *Proc. Natl. Acad. Sci.*, 2003, **100**, 2180–2184.
9 X. Yao, R. F. Henry and G. G. Z. Zhang, *J. Pharm. Sci.*, 2023, **112**, 237–242.
10 S. D. Parent, P. A. Smith, D. K. Purcell,, D. T. Smith, S. J. Bogdanowich-Knipp, A. S. Bhavsar, L. R. Chan, J. M. Croom, H. C. Bauser, A. McCalip, S. R. Byrn and A. Radocea, *Cryst. Growth Des.*, 2023, **23**(1), 320–325.
11 K. Kawakami, *J. Pharm. Sci.*, 2015, **104**, 276–279.
12 K. Kawakami, T. Harada, K. Miura, Y. Yoshihashi, E. Yonemochi, K. Terada and H. Moriyama, *Mol. Pharmaceutics*, 2014, **11**, 1835–1843.
13 K. R. Chaudhari, J. K. Savjani, K. T. Savjani and H. Shah, *Drug Dev. Ind. Pharm.*, 2021, **47**, 1633–1642.
14 C. Wang, I. Rosbottom, T. D. Turner, S. Laing, A. G. P. Maloney, A. Y. Sheikh, R. Docherty, Q. Yin and K. J. Roberts, *Pharm. Res.*, 2021, **38**, 971–990.
15 N. K. Duggirala, M. L. Perry, Ö. Almarsson and M. J. Zaworotko, *Chem. Commun.*, 2016, **52**, 640–655.
16 L. S. Reddy, S. J. Bethune, J. W. Kampf and N. Rodriguez-Hornedo, *Cryst. Growth Des.*, 2009, **9**, 378–385.
17 N. Venu, B. R. Sreekanth, T. Ram and S. Devarakonda, *Acta Crystallogr., Sect. C: Cryst. Struct. Commun.*, 2008, **64**, o290–o292.
18 S. R. Byrn, R. Pfeiffer and J. Stowell, *Solid-State Chemistry of Drugs*, SSCI Inc., West Lafayette, 2nd edn, 1999.
19 B. R. Bhogala, S. Basavoju and A. Nangia, *CrystEngComm*, 2005, **7**, 551–562.
20 A. J. Cruz-Cabeza, *CrystEngComm*, 2012, **14**, 6362–6365.
21 A. Denninger, U. Westedt, J. Rosenberg and K. G. Wagner, *Pharmaceutics*, 2020, **12**, 237–260.
22 R. I. Gelb, *Anal. Chem.*, 1971, **43**, 1110–1113.
23 P. T. Galek, F. H. Allen, L. Fábián and N. Feeder, *CrystEngComm*, 2009, **11**, 2634–2639.
24 G. M. Sheldrick, *Acta Crystallogr., Sect. A: Found. Adv.*, 2015, **71**, 3–8.
25 G. M. Sheldrick, *Acta Crystallogr., Sect. C: Struct. Chem.*, 2015, **71**, 3–8.
26 A. D. Bochevarov, E. Harder, T. F. Hughes, J. R. Greenwood, D. A. Braden, D. M. Philipp, D. Rinaldo, M. D. Halls, J. Zhang and R. A. Friesner, *Int. J. Quantum Chem.*, 2013, **113**, 2110–2142.
27 A. D. Bochevarov, M. A. Watson, J. R. Greenwood and D. M. Philipp, *J. Chem. Theory Comput.*, 2016, **12**, 6001–6019.
28 *Schrödinger Release 2022-3: MacroModel*, Schrödinger, LLC, New York, NY, 2021.
29 C. Lu, C. Wu, D. Ghoreishi, W. Chen, L. Wang, W. Damm, G. A. Ross, M. K. Dahlgren, E. Russell, C. D. Von Bargen, R. Abel, R. A. Friesner and E. D. Harder, *J. Chem. Theory Comput.*, 2021, **17**, 4291–4300.
30 C. Lee, W. Yang and R. G. Parr, *Phys. Rev. B: Condens. Matter Mater. Phys.*, 1988, **37**, 785–789.
31 J. S. Binkley, J. A. Pople and W. J. Hehre, *J. Am. Chem. Soc.*, 1980, **102**, 939–947.
32 R. A. Kendall, T. H. Dunning and R. J. Harrison, *J. Chem. Phys.*, 1992, **96**, 6796–6806.
33 C. M. Cortis and R. A. Friesner, *J. Comput. Chem.*, 1997, **18**, 1570–1590.
34 C. Wang, *PhD Thesis*, Tianjing University, 2020.
35 S. L. Morissette, O. Almarsson and S. Soukasene, Solvates and polymorphs of ritonavir and methods of making and using the same, *US Pat.*, 7205413, 2007.
36 A. Y. Sheikh, A. Mattei, R. Miglani Bhardwaj, R. S. Hong, N. S. Abraham, G. Schneider-Rauber, K. M. Engstrom, M. Diwan, R. F. Henry, Y. Gao, V. Juarez, E. Jordan, D. A. DeGoey and C. W. Hutchins, *J. Am. Chem. Soc.*, 2021, **143**, 17479–17491.